KEK Report 98-4
June 1998
M

Design and performance of a multi-element SSD for fluorescent XAFS

M. NOMURA

High Energy Accelerator Research Organization

KEK Reports are available from:

Information Resources Division
High Energy Accelerator Research Organization (KEK)
1-1 Oho, Tsukuba-shi
Ibaraki-ken, 305-0801
JAPAN

Phone: 0298-64-5137
Fax: 0298-64-4604
Cable: KEK OHO
E-mail: Library@kekvax.kek.jp
Internet: http://www.kek.jp

Design and performance of a multi-element SSD for fluorescent XAFS

NOMURA, M.
Photon Factory, Institute of Materials Structure Science, High Energy Accelerator research Organization

Abstract

A nineteen-element SSD system for fluorescent XAFS experiments was constructed, which can count up to 7 Mcps with an average energy resolution of 255 eV for Mn Kα. The dead-time correction, including that of the ICR, is derived and indicates that the dead-time due to ICR cannot be overlooked. Live time of the detection system is correctly evaluated by resetting all of the preamplifiers synchronously. By doing so, the dead-time is independent of the incoming photon energy when the gain of the spectroscopy amplifiers are adjusted so as to give a similar output pulse height. On the other hand, the dead-time depends on the output pulse height and the operation mode of the storage ring. Fluorescent XAFS spectra taken with this SSD and that with fluorescent XAFS detector are compared and the optimization of the system is discussed.

Keywords: SSD, fluorescent XAFS, dead-time correction, counting loss

I. SSD as a detector of fluorescent XAFS

Demand for structure analysis of dilute systems is increasing now. Some of such examples are dopants and impurities in materials, biological samples and environmental samples. Thin films and adsorbates on surfaces can be included in this category. Minor components and thin layers often determine the functions of materials. Thus, it is important to clarify their structure and electronic state. However, only a few methods can be used to determine the structure and electronic state of such minor components. Fluorescent XAFS is one of the most promising methods [1] for such purposes.

The minimum detection limit of fluorescent XAFS is determined by some factors. At first, the available flux is limited, by either the incoming flux or by the radiation damage of the sample. The incoming flux can be increased by using a more intense source such as an undulator or by more effective focusing optics [2], and the measurement under low temperature increases the life of the sample. Increasing the signal integrating period is commonly used. Secondary, the solid angle intercepted by the detector is limited by the size of the detector and the distance from the sample. A fluorescent ion chamber developed by Lytle *et al.* [3] is a solution, and an array of scintillation counters [4-6] is another. The signal-to-background ratio is the third limit as discussed by Warburton [7]. The signal-to-noise ratio of a spectrum can be expressed as

$$S/N = S/(S+B)^{1/2}, \quad (1)$$

where S and B indicate the signal and background including the scattering and fluorescence of coexisting elements, respectively. It is thus essential to improve the S/B ratio in order to improve the S/N ratio. Scattering x-rays are generally much more intense than the fluorescence in dilute systems. The combination of a Z−1 filter and a dispersive slit is a solution [8] to this problem. Although it is a powerful tool for fairly concentrated samples, there remains a certain limit due to the transmitting scattering x-rays, the fluorescence of coexisting atoms and that from the filter. A barrel-type crystal monochromator [9] is an ideal solution from the view point of the S/B ratio, because of its high energy resolution. However, since the detected intensity decreases significantly due to the limited acceptance angle, it cannot always improve the S/N ratio. The fourth limitation is the maximum counting rate of the detection system. With an increase of the counting rate, more pile-up occurs, which derives serious counting-loss in the detection system.

The usefulness of a solid state detector (SSD, more correct expression is semiconductor detector) was proposed by Goulding *et al.* [10] and then numerically indicated by Warburton [7]. It has a sufficiently high energy resolution to separate fluorescence signals from the scattering one. However, along with an increase of the detecting area, the capacitance of the detector increases, and thus the energy resolution decreases. Moreover, along with an increase of the counting rate, the counting loss becomes more obvious. Thus, an array of

semiconductor detectors was proposed [10]. Such arrays of semiconductor detectors were developed by Cramer *et al.* [11], Derbyshire *et al.* [12] and Oyanagi *et al.* [13].

A high energy resolution is required in order to extract a faint fluorescent signal from intense scattering and background fluorescence signals, which is essential for improving the signal-to-noise ratio, as described above. A high counting-rate capability is required at the same time in order to measure a spectrum within a reasonable period. With an increase of the input count rate, a shorter shaping time of the spectroscopy amplifier is required, which is accompanied by a deterioration of the energy resolution. Another factor limiting the counting rate is the energy rate* of the preamplifier. The current generated by detecting incoming photons causes a voltage drop across the feedback resistor in a passive preamplifier. If this voltage drop exceeds the dynamic range of the preamplifier, the preamplifier output becomes nonlinear. The maximum current can be increased by decreasing the resistance of the feedback resistor, which inevitably deteriorates the energy resolution. Reset-type preamplifiers have been developed to meet the high counting-rate requirement without seriously sacrificing the energy resolution.

The reset rate of a preamplifier is also determined by both the incoming photon flux and the photon energy. Usually, a dead-time correction is carried out while assuming that the pulse-height distribution (PHD) is independent of the counting rate. This is a good assumption in the usual diffraction experiments. However, PHD changes with the sample composition and with the energy of the primary x-ray in the case of fluorescent XAFS. Thus, a conventional system gave a different dead-time value under each experimental condition and was required to obtain a dead-time for each experiment [13]. A nineteen-element SSD with a fairly high energy resolution and high counting-rate capability has been constructed. Its performance and a simple system designed to give a unique dead-time independent of the photon energy are described.

II. Construction of the detector system

Nineteen individual pure-Ge detectors (Canberra GL0110P, 100mm^2 each, 10mm thick) are assembled in a 15-liter cryostat as shown in Figs. 1 and 2a. The distance between two neighboring elements is 14 mm. A 0.125 mm thick Be window is used to separate the vacuum environment of the cryostat from the atmosphere. Each detector is coupled to a compact pentafet preamplifier [14], which has an integrated charge restore system and is essentially a low-noise device with a short reset time. The detectors are connected to a high-voltage power supply (Canberra 3102D). The level of liquid nitrogen in the cryostat is monitored by a LN2 level monitor (Canberra 1786).

The rather conventional signal-processing system shown in Figs. 2b and 3 is adopted,

* integrated deposited energy on a detector in a second.

which consists of the following modules: 19 spectroscopy amplifiers (Canberra 2026XA), 5 single channel analyzers (SCA, Oxford TC 452), a timing pulse generator (Kinetics 3655-L1A) and 2 scalers (LeCroy 4434). All of the electronics modules are contained in three NIM-bins and a CAMAC crate. Each channel of the scaler can count up to 2^{24}= 16777216. A short shaping time, such as 0.25 μs, is usually selected in the spectroscopy amplifiers in order to meet the high counting rate. Both the SCA output and the ICR (Incoming Count Rate) pulses issued by the spectroscopy amplifiers were counted by the scalers, then transferred to a personal computer (NEC PC9801 DA7) through CAMAC. The computer also controls the other components of the beamline.

In order to evaluate the live time of the preamplifiers, two methods were considered. One was to evaluate the dwell time of each channel; the other was to reset all of the preamplifiers synchronously when a reset signal is issued by a preamplifier. The latter was adopted because of its simplicity. The timing pulse generator and scalers are also suspended during the reset period. The Kinetics 3655 CAMAC module was modified so as to realize such a function. Although the reset interval is determined by the shortest one among 19 preamplifiers, this is an economical system to evaluate the live time of preamplifiers and the same time gate can be applied to the I_0 signal. Furthermore, this system is free from any cross talk of the reset signal of the preamplifiers.

III. Performance of the detection system

Energy resolution

The energy resolution was measured with Mn Kα radiation (5.9 keV) from ^{55}Fe, whose counting rate was *ca.* 50, 50, 25, 15, 10 and 5 kcps* for a 0.25, 0.5, 1, 2, 3, 6 μs shaping time, respectively. The average energy resolution (FWHM) of nineteen detectors was 255, 217, 187, 169, 161 and 147 eV when the shaping time of the spectroscopy amplifiers was chosen to be 0.25, 0.5, 1, 2, 3, and 6 μs, respectively. The distribution of the energy resolution for each channel is shown in Fig. 4. The energy of Mn Kα is 5.9 keV, whereas that of the K absorption edge is 6.5 keV, and the energy separation between the absorption edge and fluorescence increases along with an increase of the atomic number. Therefore, the obtained resolution is sufficiently high to separate a fluorescence signal from a scattering one. This result may be changed by a reassembling of the detector element and/or an adjustment of the preamplifiers.

The variation in the energy resolution of a detector as a function of the x-ray energy was measured using fluorescence from metal foils or powder irradiated by x-rays of appropriate energies. The shaping time of the amplifier was selected to be 0.25 μs. It increased linearly with the energy of incident x-rays as shown in Fig. 5.

* kcp = 10^3 count per second.

Throughput

The throughput of the detector was evaluated by measuring the fluorescence from a copper foil, whose intensity was controlled by changing the opening of a slit placed after a focusing mirror (see Fig. 3). Since the metal foil was placed after a 1mm square receiving slit, the same area was irradiated independent of the opening of the slit after the mirror. The intensity of the primary x-ray was measured by an ionization chamber placed between the receiving slit and the sample, which should be proportional to the fluorescence intensity. The output of the ionization chamber was processed as usual and the output pulse of a voltage-to-frequency converter (VFC, 1MHz/10V) was counted by the scaler. Hereafter, the output pulse rate of the VFC is denoted as I_0. Higher orders were reduced to less than 10^{-6} of the fundamental one by detuning the double crystal monochromator installed in beamline 12C [2].

The relative throughput curves on a channel are shown in Fig. 6 as a function of the shaping time. Here, the vertical axis indicates the SCA output rate that is windowed for Cu Kα radiation, whereas the horizontal axis indicates ICR. Thus, the ratio of both axes doesn't mean the absolute throughput. The observed values (dots) were fitted well with an equation up to 400 kcps of ICR when a 0.25 μs shaping time was adopted, which indicates the high counting-rate capability of the detection system: more than 7 Mcps for nineteen channels. The details concerning the fitting equation are described in the next section.

Dead-time correction

The relative throughput curves were fitted with an equation of a first-order approximation of the paralysable and non-paralysable models [15]. This is expressed as

$$m = \beta n(1-n\tau_2), \tag{2}$$

where m is the apparent counting rate passed through an SCA window, n the ICR, τ_2 the usually used dead-time and β a proportional factor which depends on the SCA window and the PHD. This equation gave a slightly better fit than those for paralysable or non-paralysable models. The fitted curves with this equation are shown in Fig. 6 along with the observed data, which indicates that equation (2) is a good approximation up to a high counting rate. The dead-time (τ_2) obtained from the fitting was 3.1, 1.7 and 0.9 μs for a 1, 0.5 and 0.25 μs shaping time, respectively.

The ICR is usually thought to express the true incoming rate, which is a good approximation when the shaping time is long and the counting rate is not so high. However, this assumption is not exactly correct when the shaping time is short and the counting rate is very high. The ratio of ICR and I_0 was measured as a function of the counting rate. If the

response of both detection systems is ideal, the ratio should be constant independent of the ICR. However, the ratio ICR/ I_0 at ICR=400 kcps was decreased by 14 % compared with that at low counting rates as shown in Fig. 7. Therefore, the dead-time of ICR cannot be overlooked. The linearity of the ionization chamber was confirmed by other experiments. Also, if it doesn't respond linearly and the ICR responds linearly to the incoming flux, the ratio ICR/I_0 should increase along with an increase in the counting rate, which is contrary to the experimental result.

By putting the true ICR as αI_0, the apparent ICR can be expressed as

$$n = \alpha I_0 (1-\alpha I_0 \tau_1), \tag{3}$$

where I_0 is the output frequency of VFC, τ_1 the dead-time of ICR and α a proportional factor. By modifying the equation, I_0 can be approximated as

$$I_0 = n(1 + n\tau_1)/\alpha . \tag{4}$$

τ_1 was *ca.* 0.4 μs, which is not sufficiently short compared with τ_2.

Therefore, a correction of the dead-time was carried out for both τ_1 and τ_2. The true signal passed through a given SCA window (m_0) can be expressed as

$$m_0 = m (1 + n\tau_1) / (1 - n\tau_2). \tag{5}$$

Corrected counting rates both with and without the τ_1 contribution are compared in Fig. 8. The correction, excluding the dead-time of ICR (τ_1), shows a significant deviation from that including it at high counting rates, indicating the significance of the ICR dead-time.

Experimentally obtained τ_1 and τ_2 are listed in Table 1. The output pulse height is also shown in the table. The ICR is calculated by using the obtained dead-times as functions of the shaping time and counting loss rate, and is given in Table 2. This will be used as an indication to determine the shaping time of the spectroscopy amplifiers during experiments. Note that they are subject to change according to adjustments of the electronics and/or a variation in the environment. Also, it should be mentioned that the total counts (ICR), not just the SCA windowed fluorescence, limits counting rate.

Effect of a live time evaluation

In the present system, all the preamplifiers are reset synchronously and the timer and scalers are suspended during the reset period (actually longer than the reset period). The reset frequency of the preamplifiers is determined by the leakage current and by the input energy rate, which is the integrated photon energy in a unit time. Therefore, if the live times of the preamplifiers are not correctly evaluated, the dead-time for ICR (τ_1) should depend on

the incoming photon energy. This is a serious problem for fluorescent XAFS experiments, since the PHD changes at each energy according to the sample composition, especially before and after the absorption edge.

The dead-time of the ICR signal, τ_1, was compared using two kinds of characteristic radiation of different energies, Cu Kα (8.0 keV) and Mo Kα (17.4 keV) radiation; the results are compared in Fig. 9. The same shaping time, 0.25 μs, was used for spectroscopy amplifiers. The gain of the spectroscopy amplifiers was adjusted so as to give the same output pulse height for both Cu Kα and Mo Kα (*ca.* 3.9 V). The dead-time didn't change significantly, although it was anticipated qualitatively. This would be due to the shorter reset period in this system (10 μs) than estimated when the system was designed (>22 μs) [16]. When ICR was *ca.* 400 kcps, the reset frequency was *ca.* 1600 and 3000 per second for Cu Kα and Mo Kα, respectively. Thus, the dead-time due to the reset is only 1.6 and 3 % of the real time for Cu Kα and Mo Kα, respectively. Thus, the difference between these will be within the experimental error.

The author reported that the dead-time of ICR, τ_1, changed when the electronics was not suspended [17]. This result contradicts the present one. The difference in the results would be due to the fact that much longer inhibit period (87 μs) was used for suspending the electronics in the previous experiments. Thus, the dead-time due to the reset became 14 and 26 % for Cu Kα and Mo Kα, respectively.

Similar experiments were carried out by keeping a similar amplifier gain: higher output pulse height (*ca.* 7.5 V) for Mo Kα. The result is also shown in Fig. 9. A slight systematic increase of τ_2 can be observed. This is due to a difference in the response delay of SCA due to different pulse heights. However, the difference is not so large as noted in [13] and can be admitted as being within the experimental error. The reason for the scattering of τ_1 is not clear.

It is thus important to evaluate the live time of the system correctly when the reset period is fairly long. However, if it is short, a synchronous reset of all the preamplifiers and suspending the electronics during the reset period is not an inevitable method. The dead-time differs at each channel according to the adjustment of the parameters in the preamplifiers and spectroscopy amplifiers, as shown in Fig. 9.

Effect of the operation mode

The dead-time obtained from equations 2 - 5 should depend on the operation mode of the storage ring. Especially, when the storage ring is operated in the single-bunch mode it should be prominent as many photons enter the detector within a short period (100 ps), and a fairly long recovery time (0.6 μs) is kept after that. Although the stored current was about 60 mA, which is one sixth of that in the multi-bunch operation mode, more than a thirty-times intense x-ray pulse enters the detector within 100 ps every 0.6 μs at the Photon Factory. A test experiment was carried out during a single-bunch mode; the derived dead-time is

compared with those measured during the multi-bunch mode in Fig. 10. τ_1 increased from 0.28 to 0.39 μs, whereas τ_2 decreased from 1.0 to 0.91 μs in detector #10; the other channels showed a similar tendency. The dead-time value is different from those in the Table 1 and Fig. 9, since this experiment was carried out at different time with different electronics conditions. This tendency supports the above-described idea. Thus, the dead-time must be obtained for each operation mode of each storage ring. This result suggests the difficulty of dead-time correction during the hybrid mode operated at ESRF, since a multi bunch character and single-bunch character are mixed in an operation period.

IV. Comparison with a fluorescent XAFS ion chamber

A fluorescent ion chamber [3], often called as Lytle detector, is usually used for fluorescent XAFS experiments, which has a high collection efficiency of 20 % of 2π from the front of the sample. The ion chamber is usually used in combination with a filter and a diverging slit. The filter is chosen to absorb the scattering x-rays from the sample, but also to pass the fluorescence from the sample effectively. The slit is designed to maximize the throughput of the fluorescence from the sample, but as to minimize that from the filter. By combining with an appropriate filter and diverging slit, this is an economical, but powerful, tool for fairly concentrated samples : for example, more than several mmol dm^{-3} copper aqueous solution. However, with a decrease in the concentration of the interested species, the scattering and fluorescence from the filter becomes more intense than the fluorescence from the sample itself. Also, it is hard to eliminate the fluorescence from the coexisting species.

In order to compare the quality of the fluorescent spectra, 4×10^{-4} Au in silver halide was measured with both a fluorescent ion chamber and with the present multi-SSD. The signal was integrated for 3 and 10 sec. for pre- and post-edge region, respectively, in both spectra. The spectra are compared in Fig. 11. Here, a home-made fluorescent ion chamber was used, which has a longer optical path length, and thus a higher detection efficiency than the usual Lytle detector. As shown in the figure, a much lower pre-edge background signal was realized with this multi-SSD; therefore a higher S/B ratio is realized. A gallium filter ($\mu t = 6$) and dispersive slit systems were used in order to reduce the intensity of scattering. The reason for the difference in the S/B ratio between two spectra is clearly indicated in the pulse-height distribution shown in Fig. 12 (b). The integrated intensity of the scattering and fluorescence from the gallium filter is higher than that of the fluorescence from gold. The Au Lα fluorescence can be separated from the scattering, Ga Kα and Kβ fairly well when the multi-SSD is used, although all of them cannot be separated when the fluorescent ion chamber is used. Thus, a higher S/B ratio can be realized with the multi-SSD detection system.

V. Notes on taking fluorescent XAFS

It is usually thought that the quality of the fluorescent XAFS spectra is improved by using an appropriate filter and by increasing the solid angle subtended by a detector. However, this is not always correct.

The filter improves the S/B ratio of spectra when a detector which doesn't have a sufficiently high energy resolution (such as ionization chamber or scintillation counter) is used, or the detector is limited by the maximum counting rate even if it has a fairly high energy resolution. The usefulness of a filter when combined with SSD was discussed by Bilsborrow [18]. Note that the maximum counting rate was 13 kcps in [18], but 400 kcps in the present system. As indicated in the article, the filter emits its fluorescence when it absorbs the scattering x-rays. Usually Kα radiation of the filter can be easily separated from the fluorescence of the interested species when SSD is used. However, Kβ radiation of the filter element cannot be separated from the fluorescence of interest. For example, a nickel filter is used to eliminate scattering from Cu Kα. The energies of Ni Kα, Kβ and Cu Kα are 7.5, 8.3 and 8.0 keV, respectively. In this case 35% of the peak ascribable to the Cu Kα signal consists of Ni Kβ radiation because of the broadening of peaks due to the energy resolution of the SSD (270 eV) when both have the same intensity. The PHD spectra of a liver sample containing copper are compared in Figs. 13 (c) and (d), with and without a Ni filter whose μt is 3. Here, the shaping time of the spectroscopy amplifiers was set to 1 μs, and the distance between the sample and the detector was changed so that the maximum ICR becomes less than 90 kcps. Although the ratio of intensity between Cu Kα and scattering is improved by introducing the Ni filter and a slit, Ni Kβ appearing as a shoulder of Cu Kα cannot be separated, which decreases the S/B ratio in the XANES spectrum (Fig. 13 (a)) compared with that taken without the filter (Fig. 13(b)). Thus, when the sample is very dilute and the ICR is not too high, the spectrum taken without a filter gives better result.

The larger acceptance angle doesn't always result in a better S/N ratio. Fluorescence that is emitted homogeneously thus increases the fluorescent signal along with an increase in the solid angle. However, the scattering signal distributes according to $\cos^2 2\theta$ when the incident x-ray is linearly polarized, where 2θ is the scattering angle. PHD taken at the central (#10) and circumference (#01) detectors are compared in Fig. 12. Although the fluorescence is more intense than the scattering at the center (Fig.12 (a)), the situation is reversed at the circumference (Fig. 12(b)).

An example of the distribution of S/B ratio is shown in Fig. 14 according to the position of the detectors. Here, signal (S) and background (B) indicate the edge jump and the μt at pre-edge, respectively. The sample is similar to that shown in Fig. 12. The S/B ratios at the circumference detectors are rather low compared with those at the central part. In such cases better spectra may be obtained by using the data taken with the central part detectors than by using all of the detectors. Another solution is to make the distance between the

sample and the detector longer, and to choose a longer shaping time, that is to use a better energy resolution.

VI. The near future of the detection system for fluorescent XAFS

As written above, the present multi-SSD system is a powerful tool for fluorescent XAFS experiments. One problem is a difficulty of adjusting the electronics for those who are not familiar with radiation-detection systems. For example, selection of the gain and shaping time of spectroscopy amplifiers, adjusting the threshold level of pile-up-rejecters (PUR)* and the SCA window are not easy tasks for many XAFS experimenters. Recently, electronics adopting a digital signal processor in place of the conventional spectroscopy amplifier and SCA was developed by Farrow *et al.* [19, 20] in Daresbury laboratory (XSPRESS system). The XSPRESS system comprises a NIM 10MHz ADC module and a VME signal processing module for each detector. It can process as a high signal rate as the present system, and almost all of the adjustments can be done through a computer instead of adjusting the hardware manually. Furthermore, the whole PHD spectra can be recorded instead of the number of the ICR and the pulses passing through an SCA window. Thus, it is possible to draw a proper background curve by using curve-fitting, and to subtract it from the recorded signal instead of windowing by two thresholds. However, it is not possible to develop a similar system in the Photon Factory, owing to the difference in the number of specialists devoted to the development of detectors and electronics.

Fortunately, a similar electronics module (DXP/4C) is sold by XIA [21]. A DXP CAMAC module has four 20MHz ADC and can process the signals for four channels. Work to construct a fluorescent XAFS detector system using the DXP module has just started. Although the load for XAFS experimenters may decrease by using this module, that for software becomes very high and the quantity of output data becomes very large: 20 MB/spectrum.

A decrease in the electromagnetic noise is important for obtaining a better energy resolution. The environment of electromagnetic noise is different among experimental stations. For example, the noise at BL-12C is much larger than that at BL-7C, and it is difficult to discriminate electronic noise when an old passive feedback SSD is used. Thus, it is important to design and construct beamlines and experimental stations carefully in order to minimize the electromagnetic noise. The prevention of ground-loops by isolating the detector is sometimes effective. Isolation would be also effective when the detector is coupled to a vacuum chamber or the storage ring.

---

* The 2026XA spectroscopy amplifier was to adjust the threshold of PUR automatically. However, curious saturation of ICR was found during the commissioning period, which was found to be due to the improper response of automatic threshold adjustment for PUR. Thus the manual threshold adjustment was added to the circuit and it is usually used.

As indicated in a previous section, the S/N ratio of a fluorescent spectrum is determined by how well the fluorescent signal is extracted from scattering and other background fluorescence. One way is to improve the energy resolution of the detector. Two methods are considered. One is to utilize the detector which has a higher energy resolution: superconducting tunnel-junction or micro-calorimetry under an extremely low temperature. These detection systems are elegant but the cost is very high. Also it seems not to be easy to meet the high counting-rate requirement. The second method is to use a secondary spectrometer in order to separate the fluorescence from scattering etc. Although this system can provide a high energy resolution, it requires a high flux because of the limited solid angle in the spectrometer. The utilization of undulator radiation at PF-AR will solve the problem.

Acknowledgement

The author thanks Mr. Ogasawara of Toyo corporation and Mr. Tench of Canberra for their technical work, including the modification of circuits according to the author's request. The author also thanks Prof. Kazusaka of Hokkaido University for providing rat liver samples.

References

[1] J. Jaklevic, J. A. Kirby, M. P. Klein, A. S. Robertson, G. S. Brown and P. Eisenberger, *Solid State Comm.*, 23, 679 (1977).

[2] M. Nomura and A. Koyama, *KEK Report*, 95-15 (1996).

[3] F. W. Lytle, R. B. Greegor, D. R. Sandstrom, E. C. Marques, J. Wong, C. L. Spiro, G. P. Huffman and F. E. Huggins, *Nucl. Instrum. Methods*, 226, 542 (1984).

[4] S. P. Cramer and R. A. Scott, *Rev. Sci. Instrum.*, 52, 395 (1981).

[5] J. C. Phillips, *J. Phys.*, E14, 1425 (1981).

[6] H. Oyanagi, T. Matsushita, H. Tanoue, T. Ishiguro and K. Kohra, *Jpn. J. Appl. Phys.*, 24, 610 (1985).

[7] W. K. Warburton, *Nucl. Instrum. Methods*, A246, 541 (1986).

[8] E. A. Stern and S. Heald, *Rev. Sci. Instrum.*, 50, 1579 (1979).

[9] J. B. Hastings, P. Eisenberger, B. Lengeler and M. L. Perlman, *Phys. Rev. Lett.*, 43, 1807 (1979).

[10] F. S. Goulding, J. M. Jaklevic and A. C. Thompson, *SSRL Report*, 78/04, II-22 (1978).

[11] S. P. Cramer, O. Tench, M. Yocum and G. N. George, *Nucl. Instrum. Methods*, A266, 586 (1988).

[12] G. E. Derbyshire, A. J. Dent, B. R. Dobson, R. C. Farrow, A. Felton, G. N. Greaves, C. Morrell and M. P. Wells, *Rev. Sci. Instrum.*, 63, 814 (1992).

[13] H. Oyanagi, M. Martini and M. Saito, *Nucl. Instrum. Methods*, A403, 58 (1998).

[14] T. Nashashibi, *Nucl. Instrum. Methods*, A322, 551 (1992).

[15] K. Zhang, G. Rosenbaum and G. Bunker, *Jpn. J. Appl. Phys.*, Suppl. 32-2, 147 (1993).

[16] C. L. Briton, T. H. Becker, T. J. Paulus and R. C. Tranmell, *IEEE Trans. Nucl. Sci.*, NS-31, 455 (1984).

[17] M. Nomura, *J. Synchrotron Radiation*, in press.

[18] R. Bilsborrow, *Rev. Sci. Instrum.*, 63, 890 (1992).

[19] R. Farrow, G. E. Derbyshire, B. R. Dobson, A. J. Dent, D. Bogg, J. Headspith, R. Lawton, M. Martini, R. Trammell and K. Buxton, *Rev. Sci. Instrum.*, 66, 2307 (1995).

[20] R. Farrow, G. E. Derbyshire, B. R. Dobson, A. J. Dent, D. Bogg, J. Headspith, R. Lawton, M. Martini, K. Buxton and R. Trammell, *Physica*, B208 &209, 256 (1995).

[21] W. K. Warburton, User's manual of digital x-ray processor model 4C/4T (DXP-4C/4T).

Table 2. Calculated ICR/cps as functions of the counting loss rate and the shaping time of the spectroscopy amplifier. Here, τ_1 obtained from 0.25 μs is applied for all shaping time.

		shaping time/μs					
		0.25	0.5	1	2	3	6
Dead-time	τ_1/μs	0.41	0.41	0.41	0.41	0.41	0.41
	τ_2/μs	0.89	1.66	3.1	6.3	9.2	18.4
Counting loss rate	5 %	39k	24k	14k	7k	5k	3k
	10 %	79k	49k	29k	15k	10k	5k
	20 %	164k	101k	58k	30k	21k	11k
	30 %	255k	154k	89k	46k	32k	16k
	40 %	352k	210k	120k	61k	42k	21k

This table means that if a 0.25 μs shaping time is used and a 30 % counting loss is allowed, each detector can count up to 255 kcps as ICR.

Table 1. Experimentally obtained dead-time, τ_1 and τ_2, for each detection channel. The detector #04 was not functioning well.

shaping time	0.25 μs		0.5 μs		1 μs		2 μs		3 μs		6 μs	
Detector #	τ_1	τ_2	τ_1	τ_2	τ_1	τ_2	τ_1	τ_2	τ_1	τ_2	τ_1	τ_2
1	0.31	0.90	0.29	1.70	0.30	3.16	0.21	6.44	0.28	9.15	0.44	18.32
2	0.66	0.93	0.62	1.71	0.57	3.12	0.50	6.39	0.59	9.16	0.82	18.01
3	0.41	0.90	0.39	1.66	0.39	3.09	0.47	6.32	0.38	9.23	0.16	18.55
4												
5	0.34	0.89	0.32	1.74	0.31	3.12	0.38	6.29	0.35	9.24	0.33	18.33
6	0.53	0.84	0.47	1.65	0.44	3.07	0.51	6.22	0.47	9.22	0.77	18.87
7	0.47	0.93	0.44	1.69	0.42	3.11	0.33	6.16	0.42	9.11	0.47	18.24
8	0.40	0.92	0.43	1.66	0.45	3.20	0.35	6.45	0.31	9.08	0.47	18.37
9	0.47	0.91	0.46	1.67	0.45	3.08	0.55	6.24	0.43	9.11	0.71	18.22
10	0.44	0.92	0.42	1.70	0.39	3.07	0.53	6.34	0.42	9.37	0.40	18.65
11	0.34	0.88	0.30	1.67	0.28	3.08	0.42	6.23	0.30	9.17	0.58	18.18
12	0.54	0.87	0.52	1.60	0.44	3.07	0.55	6.24	0.50	9.23	0.60	18.49
13	0.32	0.87	0.30	1.68	0.28	3.11	0.35	6.33	0.33	9.21	0.68	18.36
14	0.33	0.88	0.30	1.64	0.30	3.07	0.38	6.14	0.30	9.09	0.34	18.43
15	0.35	0.87	0.33	1.62	0.29	3.10	0.34	6.36	0.31	9.23	0.38	18.56
16	0.37	0.86	0.35	1.63	0.32	3.08	0.40	6.25	0.38	9.20	0.53	18.97
17	0.39	0.90	0.39	1.60	0.37	3.08	0.38	6.28	0.42	9.32	0.54	18.40
18	0.34	0.86	0.31	1.59	0.29	3.09	0.21	6.34	0.22	9.14	0.46	18.02
19	0.38	0.89	0.35	1.63	0.32	3.11	0.42	6.40	0.33	9.37	0.44	18.18
Average	0.41	0.89	0.39	1.66	0.37	3.10	0.41	6.30	0.38	9.20	0.51	18.40
St. Dev.	0.09	0.03	0.09	0.04	0.08	0.03	0.10	0.09	0.09	0.09	0.17	0.26
pulse height	3.9 V		4.4 V		4.4 V		4.5 V		4.5 V		4.5 V	

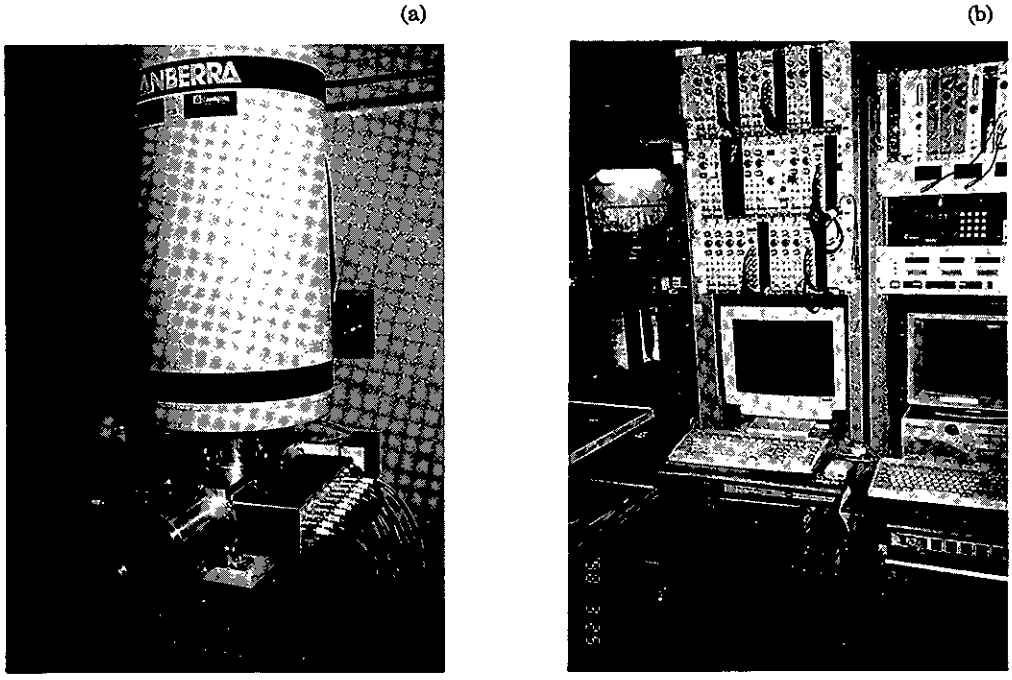

Fig.2. Photograph of the nineteen-element SSD (a) and the signal processing electronics(b). A card-type multi-channel analyzer (Labo MCA/PC98BX) is placed in the microcomputer.

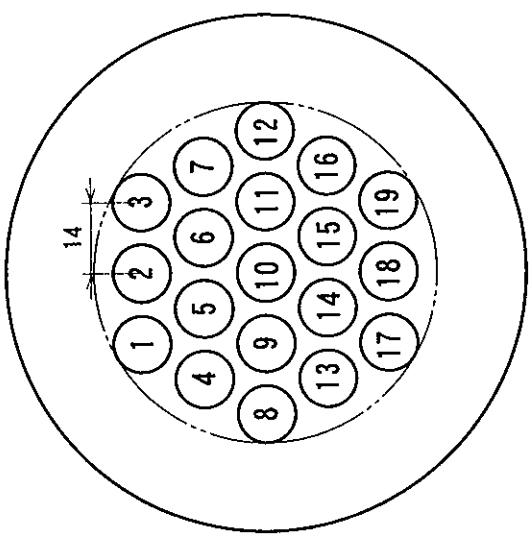

Fig.1. Arrangement of 19 detectors. The area of each element is 100 mm^2 and is separated from the neighboring one by 14 mm.

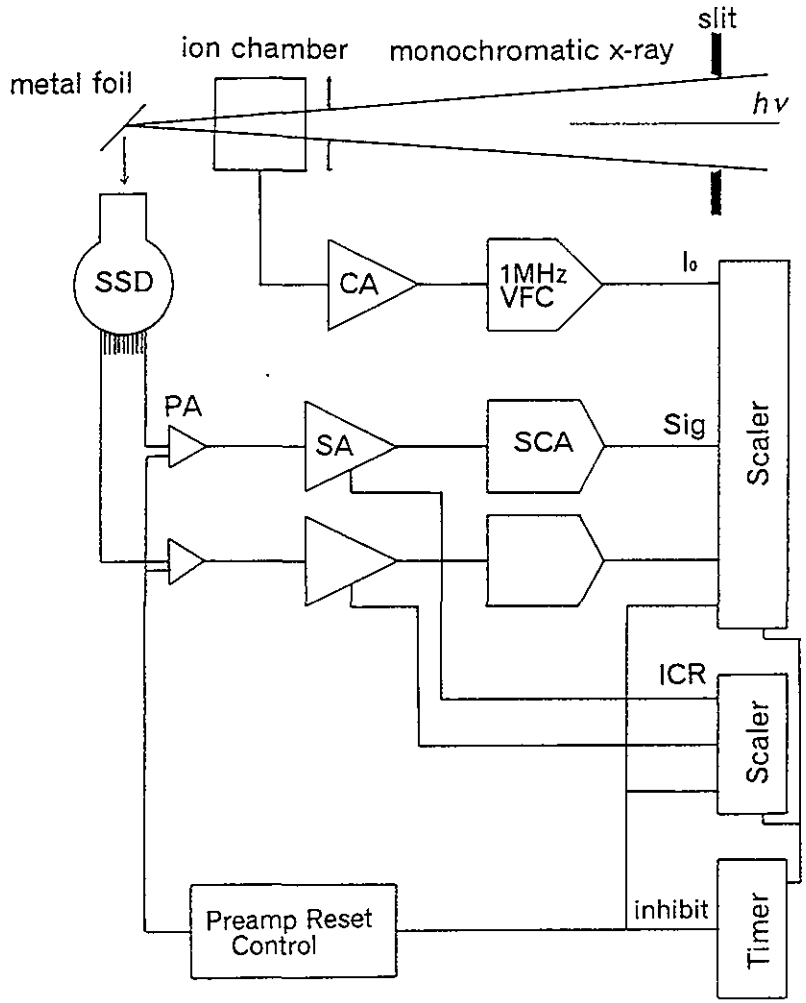

Fig.3. Schematic drawing of the setup used for the dead-time measurement including the signal processing system. The incoming flux is controlled by the slit and the intensity is monitored by an ionization chamber. The current is amplified by a current amplifier (CA), then converted to a pulse train by a voltage-to-frequency converter (VFC). Fluorescence from a metal foil is detected by an array of SSD, amplified by preamplifiers (PA) and spectroscopy amplifiers (SA) then energy analyzed by single-channel-analyzers (SCA). Both output pulses from SCA and ICR issued by the spectroscopy amplifiers are counted by the scalers during the period defined by the timer.

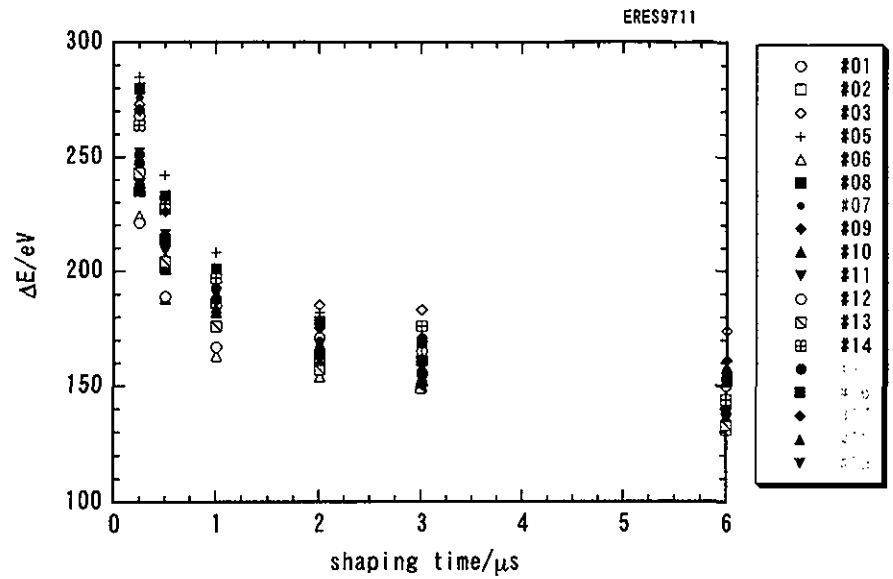

Fig.4. Energy resolution of each detector as a function of the shaping time of the spectroscopy amplifiers. The result may be changed by reassembling the detectors and/or adjusting the preamplifiers.

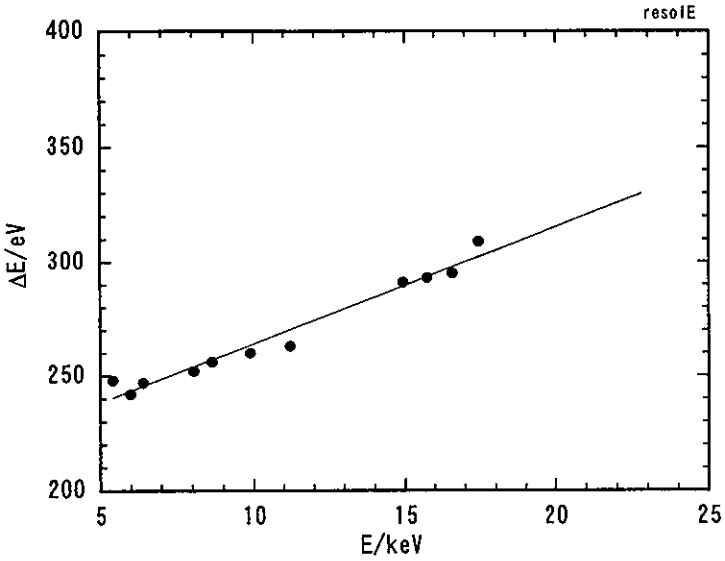

Fig. 5. Energy resolution of a detector as a function of the incident x-ray energy. The shaping time of the amplifier was 0.25 μs.

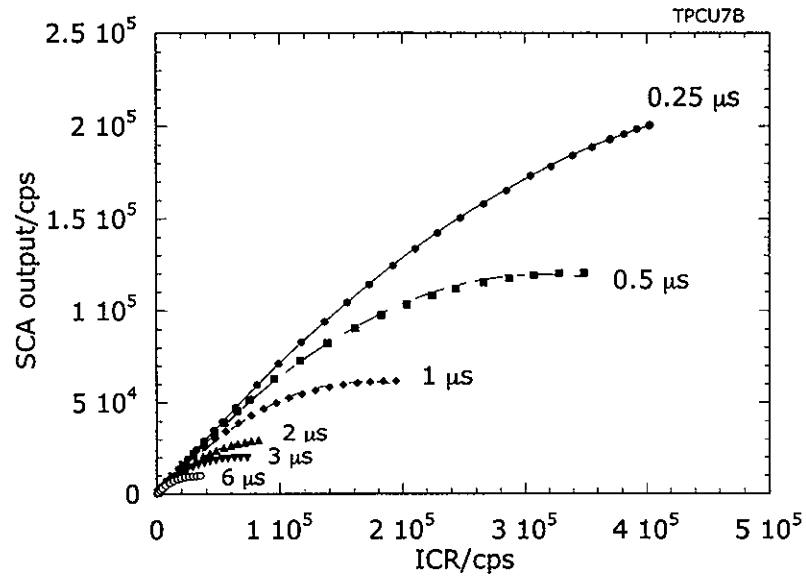

Fig. 6. Relative throughput curves as functions of the shaping time and ICR. Here, the vertical axis is the signal rate passed through an SCA which is windowed for Cu Kα. The dots are the observed data and the lines are least-squares fittings using eq. 2. The system can count up to 400 kcps for each channel when the shaping time is adjusted to 0.25 μs.

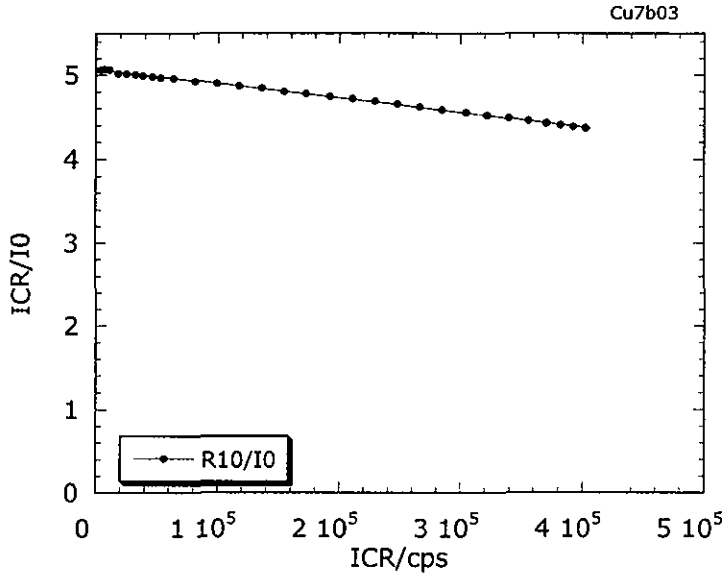

Fig. 7. ICR/I_0 as a function of ICR. If both I_0 and ICR are linear, it should be constant independent of the ICR.

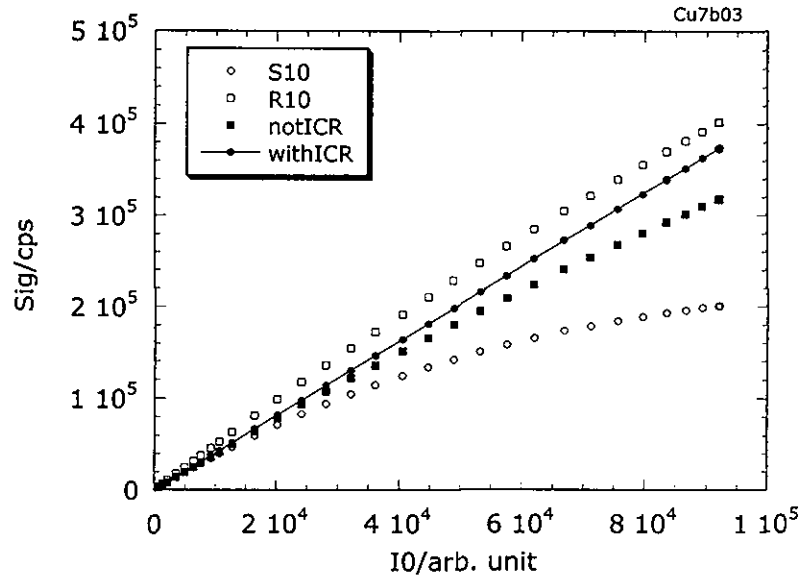

Fig. 8. Response of the output signal from an SSD as a function of the incoming flux. The raw SCA output (○), raw ICR (□), dead-time corrected SCA output according to eq. 4 (●) and that according to eq. 1 (■) are plotted. Only the closed circles show a linear response to I_0, as indicated by the straight line, indicating the significance of the dead-time in ICR.

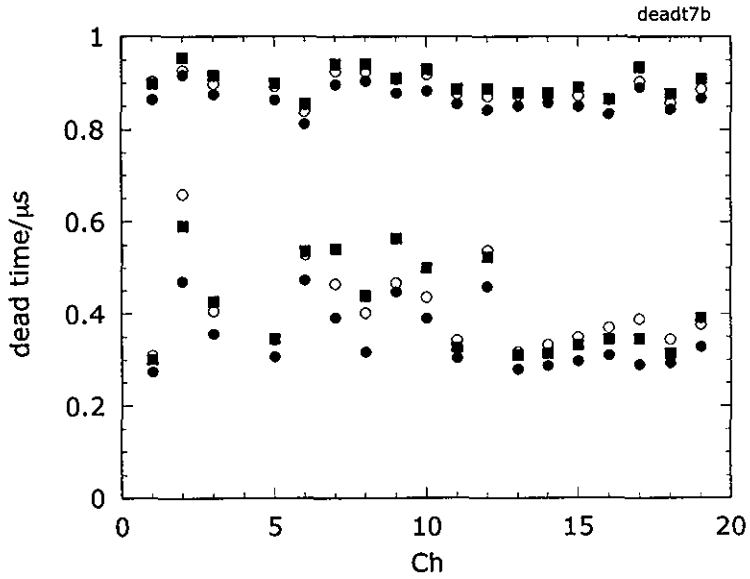

Fig. 9. Dead-times obtained for each channel when the condition of the photon and the condition of the electronics are changed. The closed marks were obtained from Mo Kα (17.4 keV) and the open ones from Cu Kα (8 keV). Spectroscopy amplifiers were adjusted so as to give the same output pulse height (○, ●, *ca.* 3.9 V), whereas a similar amplifier gain and a higher pulse height (*ca.* 7.5 V) was used for ■.

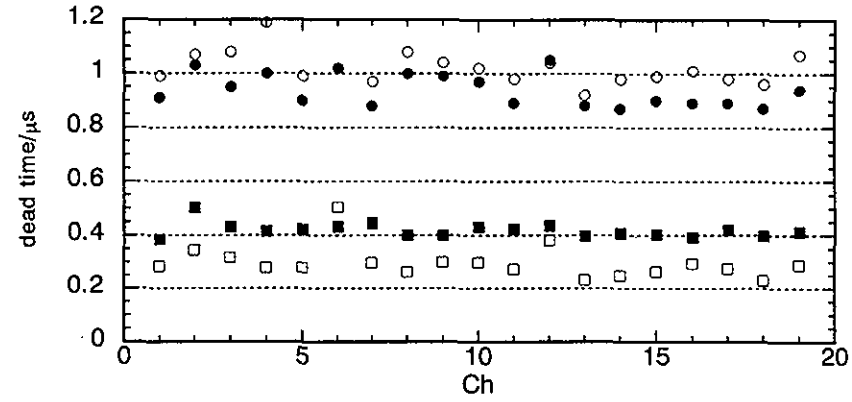

Fig. 10. Dead-time obtained during the multi-bunch operation mode (○) and during the single-bunch mode (●). A clear difference in the dead-time can be seen.

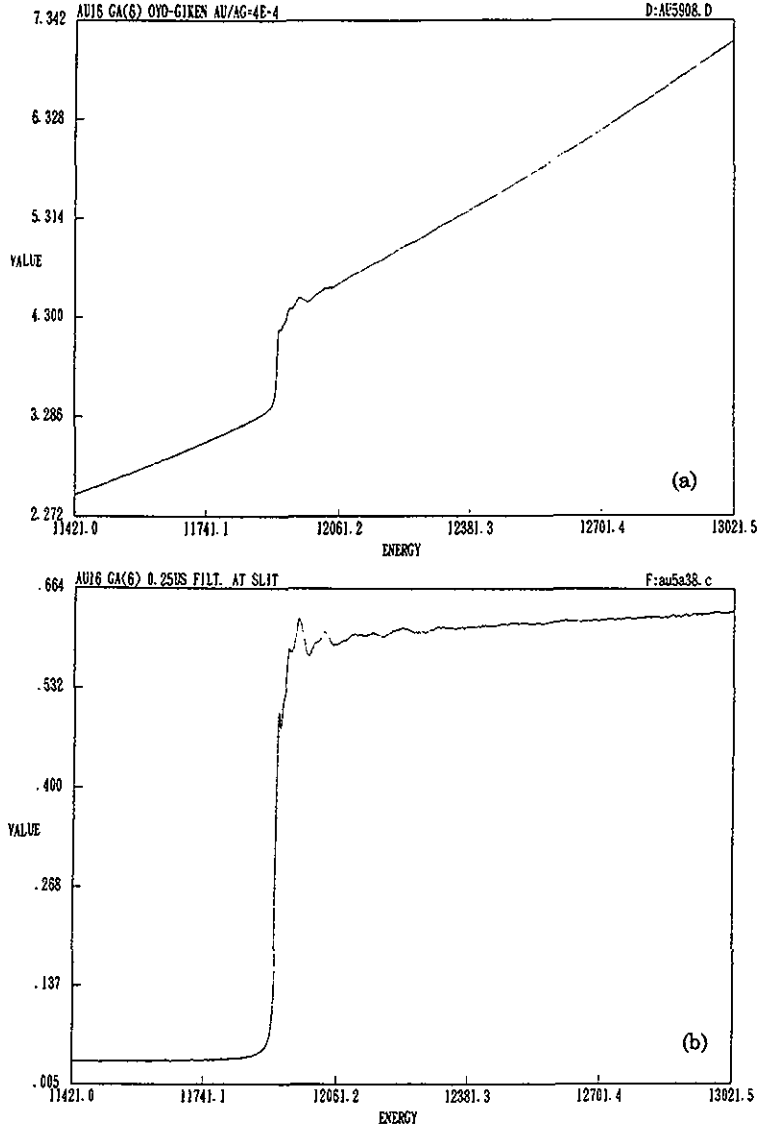

Fig. 11. Fluorescent XAFS spectra of 4×10^{-4} Au in a silver halide taken with fluorescent ion chamber (a) and the multi-SSD (b). The background in the pre-edge region is much lower in (b) than in (a). The elastic scattering was reduced by using a Ga(6) filter and dispersing slits.

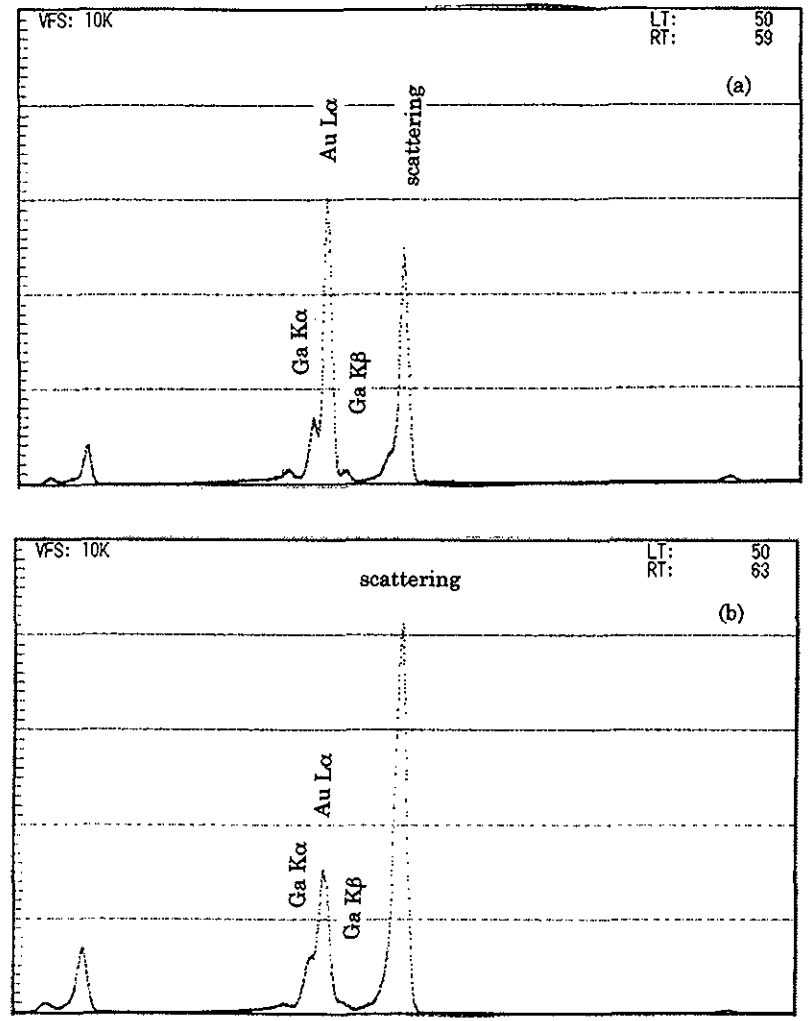

Fig. 12. Pulse-height distribution spectra measured at the central detector #10 (a) and the surrounding one #01(b). Assignments of the peaks are shown in the figure. The Ga fluorescence comes from the filter used to reduce the scattering x-rays.

Fig. 13. Fluorescent XAFS spectra of liver tissue containing copper taken with (a) and without (b) a Ni filter, whose absorbance is 3. The PHD corresponding to (a) and (b) are shown in (c) and (d). Although the Cu Kα/scattering ratio increases with the Ni filter, the S/B ratio of the fluorescent XAFS spectrum decreases, owing to the overlap of Cu Kα and Ni Kβ emitted from the filter.

CU6608.CUM

4.4 5.7 4.9
5.6 8.0 9.5 4.9
4.6 9.1 14.3 7.9 5.7
5.7 8.1 9.0 6.4
3.6 6.8 4.3

Fig. 14. Distribution of the S/B ratio among nineteen channels. Here, S and B indicates the edge jump and the pre-edge absorbance, respectively.